Paper No. 188. (quote when citing this article)
Eleventh World Conference on Earthquake Engineering
ISBN: 0 08 042822 3

ULTIMATE TENSILE STRENGTH OF 780MPa-GRADE HIGH-QUALITY STEEL PLATES JOINTED WITH HIGH-STRENGTH BOLTS

KUNIAKI UDAGAWA,[1] TAKAO YAMADA[2] and ANWER YASIN[3]

[1]Dept. of Architecture, Tokyo Denki Univ., 2-2 Nishiki-cho, Kanda, Chiyoda-ku, Tokyo 101, JAPAN
[2]NKK Technology, Development of Building and Construction Dept., 1-1-2 Marunouchi, Chiyoda-ku, Tokyo 100, JAPAN
[3]Computer Science Dept., Xinjiang Institute of Technology, No. 21 North Friendship Road, Urumuqi, PEOPLE'S REPUBLIC OF CHINA

ABSTRACT

We investigate the ultimate tensile strength of 780MPa-grade high-quality steel plates jointed with high-strength bolts experimentally. We propose formulas to predict the ultimate tensile strength of the joint plates for three failure modes: net section fracture, tearing fracture and end fracture. The experimental results confirm the validity of the formulas. Also, the minimum edge distance necessary to ensure an axial yield force in the tension members is discussed.

KEYWORDS

780MPa-grade high-quality steel; high-strength bolt; joint plate; bolt-hole arrangement; tension test; ultimate strength; failure mode; prediction formula

INTRODUCTION

Many feasibility studies have been performed to determine the applicability of newly developed 780MPa (tensile strength)-grade high-quality steel, which has a low yield ratio, to supertall buildings. In order to use 780MPa-grade high-quality steel (hereafter referred to as 780MPa-grade steel, or HQ780 in the figures and one table) for tension members jointed with high-strength bolts, it is essential to understand the plastic behavior of these joints. The ultimate strength design must be such that tension members jointed with high-strength bolts do not break at the joint before the plastic deformation of the tension members reaches a certain level. In this context, we investigated the ultimate tensile strength of 780MPa-grade steel plates jointed with high-strength bolts experimentally. It is known that there are three failure modes for steel joint plates: net section fracture, tearing fracture and end fracture. The effects of bolt-hole arrangement and edge distance of the bolted joints on the ultimate strength of the joint plates and the failure mode were investigated.

We proposed formulas to predict the ultimate tensile strength of joint plates on the basis of the experimental results. In addition, the experimental results were compared with the design values specified in the "Standard for Limit State Design of Steel Structure (draft)" (LSD) (Architectural Institute of Japan, 1992) and the "Load and Resistance Factor Design Specification for Structural Steel Buildings" (LRFD) (American Institute of Steel Construction, 1986). The ultimate strengths in these specifications are for 400MPa-grade or 490MPa-grade steel joint plates. We assessed the adaptability of the LSD and LRFD design formulas to 780MPa-grade steel joint plates.

Relationships between the failure modes and the geometric properties of the bolt-hole arrangements were clarified. Furthermore, a minimum edge distance measured perpendicular to the force line of the bolt holes was discussed based on experimental data, under the condition that the distance ensured the ultimate strength grater

than the axial yield force of the tension members. In this study, tension tests on 400MPa-grade steel joint plates were also conducted in order to compare the prediction formulas for 400MPa-grade steel (referred to as SS400 in the figures and one table) joint plates with those for 780MPa-grade steel joint plates. Finally, the reliability of the LSD and LRFD design formulas was discussed based on the test results for the 400MPa-grade steel joint plates.

EXPERIMENT

Test Specimens

As mentioned above, the failure modes of steel joint plates are net section fracture, tearing fracture and end fracture as shown in Fig. 1. Tearing fracture includes inner and outer tearing fractures. The failure mode depends on the geometric properties of the joint plate, which are determined by the bolt-hole arrangement, the edge distances e_1 and e_2 measured parallel and perpendicular to the force line, respectively, and the gage distance g of the bolt holes. A test specimen with a bolt-hole arrangement of 2 rows and 3 lines (hereafter referred to as 2×3) is shown in Fig. 2. A total of 73 780MPa-grade steel joint plates, 12 mm thick, were tested. The following bolt-hole arrangements were used: 1×2, 1×3, 1×4, 2×2, 2×3, 2×4, 3×2, 3×3, 4×2 and 4×3. Ultrahigh-strength bolts (M16) made of maraging steel were used to avoid bolt breakage in the tests. The diameter and pitch of the bolt holes were 18 mm and 40 mm, respectively. The edge and gage distances of each specimen are shown in Table 1, in which the first and second numbers of the specimen's name show the numbers of rows and lines, respectively. d denotes a bolt diameter of 16 mm. Tension tests were carried out on 400MPa-grade steel joint plates with bolt-hole arrangements similar to those of the 780MPa-grade steel joint plates in order to investigate the difference between the 780MPa-grade steel and 400MPa-grade steel joint plates.

Material Properties

Table 2 shows the yield points, tensile strengths, yield ratios and elongation factors at the breakage obtained from coupon tests on the 780MPa-grade steel plates. The yield points were determined by the 0.2% offset method. The 780MPa-grade steel used in these tests is different from the current 780MPa high-tension steel, and has a low yield ratio. Japanese steel makers specify a yield point in the range of 6.30 to 7.25 t/cm^2, a tensile strength in the range of 7.60 to 8.80 t/cm^2, a yield ratio of less than 0.85 and an elongation factor at breakage of more than 0.16. Although some of the 780MPa-grade steel plates did not meet the specifications, the test results for these plates are included in the discussion section. The material properties of the 400MPa-grade steel plates are also shown in Table 2.

Loading and Measurement

The apparatus used for the tension tests is shown in Fig. 3. The tests were conducted under nonfriction conditions at the high-strength bolt joints in order to evaluate the ultimate strength accurately. The tensile load P and axial deformation δ of a section of length l_0 were measured as shown in Fig. 3.

EXPERIMENTAL RESULTS

The relationships between tensile load and axial deformation for each fracture type are shown in Fig. 4. Photo 1 shows specimens fractured in each of the three modes. Table 1 shows the ultimate strength ePui and fracture type of each specimen. Failure modes I, II, III and IV in the table designate net section fracture, inner tearing fracture, outer tearing fracture and end fracture, respectively.

DISCUSSION

Prediction of Ultimate Strength for Four Fracture Types

We predicted the ultimate strengths of the joint plates for each type of fracture based on the experimental results. The prediction formulas were

net section fracture $\quad c P u1 = \beta \sigma_u A e \qquad (1)$

inner tearing fracture $\quad c P u2 = \alpha_2 \sigma_u A ns + \beta \sigma_u A nt \qquad (2)$

outer tearing fracture $cPu3 = \alpha_3\sigma_u Ans + \beta\sigma_u Ant'$ (3)
end fracture $cPu4 = \alpha_4\sigma_u Ans \cdot m.$ (4)

Section areas *Ae*, *Ans*, *Ant* and *Ant'* are shown in Fig. 2. β in Eq. 1 is defined as the increase coefficient of tensile strength, since, in the case of net section fracture, the restriction of plate deformation due to the bolts increases the tensile strength at the net section. Assuming a uniform increase in tensile strength at the net section, the increase coefficient for each specimen was obtained under the condition that the experimental ultimate strength $ePu1$ for each specimen undergoing net section fracture was equal to $\beta\sigma_u Ae$. Figure 5 shows relationships between β and $Ant'/Ant(m\text{-}1)$. Here, m indicates the number of rows. Figure 5 shows that the values of β for specimens with 2 rows of holes are grouped together, as are those for specimens with 3 and 4 rows of holes. β is given by the following regression lines as a function of $Ant'/Ant(m\text{-}1)$ for each group.

2 rows $\beta = 1.120 - 0.027 Ant'/Ant(m\text{-}1)$ (5)
3 and 4 rows $\beta = 1.146 - 0.019 Ant'/Ant(m\text{-}1)$ (6)

α_2–α_4 in Eqs. 2 – 4 are defined as the shear strength coefficients. For example, the coefficient α_2 for each specimen undergoing inner tearing fracture was calculated under the condition that the experimental ultimate strength $ePu2$ is equal to $\alpha_2\sigma_u Ans+\beta\sigma_u Ant$. Here, the values given by the regression lines in Eqs. 5 and 6 were adopted for β. The relationships between α_2 and l/d for each specimen are shown in Fig. 6(a). l is shown in Fig. 2. The shear strength coefficients α_3 and α_4 for outer tearing fracture and end fracture are obtained in the same manner. The relationships between α_3 and l/d, and those between α_4 and l/d are shown in Figs. 6(b) and 6(c), respectively. The regression lines of the relationships between α_i ($i = 2 - 4$) and l/d for each fracture type are expressed as

inner tearing fracture $\alpha_2 = 0.5054 - 0.0088 l/d$ (7)
outer tearing fracture $\alpha_3 = 0.4333 + 0.0040 l/d$ (8)
end fracture $\alpha_4 = 0.5156 - 0.0143 l/d.$ (9)

The ultimate strengths $cPui$ predicted using the formulas (Eqs. 1–4) are obtained using the above regression lines for β and α_i. The experimental $ePui$ and predicted $cPui$ values of the ultimate strengths were compared, as shown in Fig. 7. The predicted ultimate strengths agreed well with those obtained experimentally. The experimental and predicted ultimate strengths for the 400MPa-grade steel joint plates were obtained in the same way as those for the 780MPa-grade steel plates. The results for the 400MPa-grade steel specimens are also given in Fig. 7.

Ultimate Strength Specified in LSD and LRFD

Design formulas for the ultimate strength for inner tearing fracture have been proposed in the LSD of the Architectural Institute of Japan and the LRFD of the American Institute of Steel Construction. The design value in the LSD was the smaller of the two values obtained from Eqs. 10 and 11. The larger of the two values obtained from Eqs. 12 and 13 is that specified in the LRFD. The four section areas (*Ant*, *Ans*, *Avg* and *Atg*) in Eqs. 10 - 13 are shown in Fig. 8.

LSD $\sigma_u Ant + \sigma_y/\sqrt{3} Ans$ (10)
LSD $\sigma_y Ant + \sigma_u/\sqrt{3} Ans$ (11)
LRFD $0.6\sigma_y Avg + \sigma_u Ant$ (12)
LRFD $0.6\sigma_u Ans + \sigma_y Atg$ (13)

The ultimate strengths of the test specimens in this study were predicted using these design formulas under the assumption that the design formulas were adaptable to 780MPa-grade steel plates. These values are compared with the experimental ultimate strengths in Figs. 9(a) and 9(b). In the same manner, the ultimate strengths of 400MPa-grade steel specified in the LSD and LRFD and those obtained experimentally are compared in Figs. 9(c) and 9(d). There was less difference between the design and experimental ultimate strengths for 780MPa-grade steel than between the design and experimental values for 400MPa-grade steel. The design values calculated using the LSD formula for both 780MPa- and 400MPa-grade steel specimens were lower than the experimentally obtained values. Most of the design values calculated using the LRFD formula were higher for the 780MPa-grade steel specimens and lower for the 400MPa-grade steel specimens than the experimentally obtained values. In the case of the 400MPa-grade steel plates, the design formulas in the LRFD gave better predictions than those in the LSD. With regard to the 780MPa-grade steel plates, the design values in the LSD approached the experimental values and those in the LRFD exceeded them, since the yield ratio of the 780MPa-grade steel was greater than that of the 400MPa-grade steel.

Failure Modes and Geometric Properties of Joint Plates

If the bolt arrangement of a joint plate is determined, four ultimate strengths can be calculated using the prediction formulas for the four fracture types. Actual fracture occurs at the lowest of the four ultimate strengths. If the geometric properties of the joint plates are known, the fracture type can be determined. A fracture domain diagram, which shows the relationships between the failure modes and the geometric properties, was drawn using the four prediction formulas. The fracture domain for each type of fracture is shown in Fig. 10 with $An't/An$ on the x axis and $An s/An$ on the y axis. This domain diagram is for a joint plate with a 2×3 bolt-hole arrangement. The fracture type determined from the fracture domain diagram on the basis of the geometric properties of the specimen was the same as that observed in the test in each case.

Minimum Edge Distance and Axial Yield Force of Gross Area

Using specimens which underwent net section fracture, the ratios of the experimental ultimate strength to the axial tensile yield force (gross area of steel plate Ag times yield stress σ_y) were calculated. Relationships between the edge distance e_2/d and the ratio $ePu1/Ag\sigma_y$ for the specimens with a gage distance of $2.5d$ are shown in Fig. 11. Results for both 780MPa-grade steel and 400MPa-grade steel joint plates are given. The ultimate strength of all of the 780MPa-grade steel joint plates was less than the axial tensile yield force in the present test. Furthermore, as the numbers of rows increased, the difference between the ultimate strength and the axial tensile yield force increased. In the case of high-strength steel joint plates, in order to ensure that the ultimate strength is greater than the axial tensile yield force, it is necessary to increase the gage distance g. However, the relationship between the gage distance g and the distance e_2 must be taken into account in this evaluation.

Ductility Factors of Joint Plates

The ductility factors $\delta_m/\varepsilon_y l_0$ for each specimen are shown in Fig. 12. Here, δ_m is defined as the axial deformation at the ultimate strength. ε_y denotes the yield strain, and l_0 is the length of the test section undergoing axial deformation as shown in Fig. 3. The ductility factors of the 400MPa-grade steel specimens are also shown in Fig. 12. For specimens undergoing end fracture, the ductility factors of the 780MPa-grade steel joint plates were smaller than those of the 400MPa-grade steel joint plates, but the range of values was not very large. In the case of net section, inner tearing, and outer tearing fractures, the ductility factors of the 780MPa-grade steel joint plates were much smaller than those of the 400MPa-grade steel joint plates, differing by a factor of 5 or 6.

CONCLUSIONS

From the results of tension tests on high-strength bolted joint plates made of 780MPa-grade steel and 400MPa-grade steel, the following conclusions have been obtained. 1) Formulas for the prediction of the ultimate strength of joint plates with high-strength bolts were proposed for four types of fracture. Values of the ultimate strength predicted using the formulas agreed with those obtained experimentally. There was little difference between the coefficients in the formulas for 780MPa-grade and 400MPa-grade steel plates. 2) Comparing the values calculated using the design formulas in the LSD and LRFD to the experimental results, the LSD formula gave smaller values for both 780MPa-grade steel and 400MPa-grade steel joint plates. The LRFD formula underestimated the ultimate strengths of 400MPa-grade steel joint plates and overestimated those of 780MPa-grade steel joint plates. 3) The relationships between the failure modes and the geometric properties of the joint plates were clarified. Fracture domain diagrams determined by the geometric properties were obtained. These diagrams enabled us to predict the type of fracture which would develop in a specimen with given geometric properties. 4) To ensure the ultimate strength greater than the axial yield force in the tension member, the minimum edge distance measured perpendicular to the force line, which varied with the properties of the steel, was clarified. 5) The axial ductility factors of the 780MPa-grade steel joint plates were one-fifth to one-sixth of those of the 400MPa-grade steel joint plates in the case of net section, inner tearing and outer tearing fractures.

REFERENCES

Architectural Institute of Japan (1992). Standard for Limit State Design of Steel Structure (draft).
American Institute of Steel Construction (1986). Load and Resistance Factor Design Specification for Structural Steel Buildings.

Table 1 Geometric properties of specimens and test results.

Specimen	e_1/d	e_2/d	g/d	${}^eP_{ui}(t)$	Failure Mode
121	0.95	7.53	-	45.8	Ⅳ
122	1.47	7.52	-	54.2	Ⅳ
123	1.97	7.52	-	63.0	Ⅳ
124	2.48	7.52	-	69.4	Ⅳ
131	1.02	7.50	-	77.2	Ⅳ
132	1.27	7.50	-	80.9	Ⅳ
133	1.53	7.50	-	83.8	Ⅳ
134	1.95	7.52	-	88.5	Ⅳ
135	2.47	7.50	-	96.6	Ⅳ
141	0.96	7.52	-	91.6	Ⅳ
142	1.45	7.51	-	100.4	Ⅳ
143	1.99	7.52	-	107.0	Ⅳ
144	2.47	7.52	-	114.6	Ⅳ
221	1.49	6.26	2.50	75.4	Ⅱ
222	2.48	6.26	2.50	94.5	Ⅱ
223	1.46	5.51	4.00	98.4	Ⅱ
224	2.48	5.53	4.00	118.6	Ⅱ
231	4.07	0.98	2.48	39.4	Ⅰ
232	4.05	1.22	2.50	46.4	Ⅰ
233	4.00	2.00	2.50	70.7	Ⅰ
234	4.00	2.50	2.53	85.6	Ⅰ
235	4.06	0.99	4.00	65.2	Ⅰ
236	4.00	1.25	4.00	73.1	Ⅰ
237	4.06	1.99	4.02	99.0	Ⅰ
238	4.05	2.48	4.02	114.5	Ⅰ
239	4.02	0.96	5.04	81.7	Ⅰ
23A	4.00	1.25	5.03	89.8	Ⅰ
23B	4.06	1.99	4.99	115.9	Ⅰ
23C	4.04	2.51	5.04	131.8	Ⅰ
23D	1.50	5.67	7.48	177.4	Ⅳ
23E	1.50	6.25	2.50	107.5	Ⅱ
23F	2.49	6.28	2.49	127.1	Ⅱ
23G	1.19	5.51	3.99	130.8	Ⅱ
23H	2.50	5.50	4.00	151.3	Ⅱ
23I	1.19	5.02	4.98	144.4	Ⅱ
23J	2.50	5.00	5.03	167.6	Ⅱ

Specimen	e_1/d	e_2/d	g/d	${}^eP_{ui}(t)$	Failure Mode
23K	1.21	1.46	11.99	123.7	Ⅲ
23L	2.48	1.51	11.99	142.3	Ⅲ
23M	2.46	2.48	12.00	162.6	Ⅲ
23N	1.20	3.75	7.50	162.5	Ⅳ
23P	2.50	3.79	7.49	200.0	Ⅳ
241	1.47	5.50	4.01	154.0	Ⅱ
242	2.48	5.51	3.99	173.6	Ⅱ
243	1.47	5.01	5.00	170.8	Ⅱ
244	1.46	1.36	11.99	149.2	Ⅲ
245	2.49	1.40	12.00	164.4	Ⅲ
246	2.47	2.43	12.00	198.4	Ⅲ
321	1.47	5.01	2.50	96.0	Ⅱ
322	2.48	5.01	2.50	115.4	Ⅱ
323	1.98	4.02	4.00	153.8	Ⅱ
324	2.45	4.00	4.00	160.6	Ⅱ
325	1.48	2.51	4.00	142.2	Ⅱ
326	2.47	2.49	3.99	128.0	Ⅲ
331	1.98	0.99	2.49	59.4	Ⅰ
332	1.97	1.49	2.50	74.1	Ⅰ
333	1.98	2.02	2.50	90.0	Ⅰ
334	1.98	3.01	2.50	117.2	Ⅰ
335	2.48	1.50	4.00	123.6	Ⅰ
336	1.46	5.03	2.50	126.8	Ⅱ
337	1.47	4.53	4.00	168.4	Ⅱ
338	0.98	1.52	4.00	108.8	Ⅲ
421	1.48	1.48	4.00	166.8	Ⅰ
422	2.49	3.77	2.51	136.6	Ⅱ
423	1.49	3.75	2.52	115.8	Ⅱ
424	2.46	1.48	4.00	101.4	Ⅲ
431	1.97	1.02	2.50	83.4	Ⅰ
432	1.98	1.52	2.50	100.8	Ⅰ
433	1.98	1.99	2.50	113.8	Ⅰ
434	1.98	3.03	2.50	143.2	Ⅰ
435	3.98	4.03	2.50	171.2	Ⅰ
436	1.46	1.50	3.99	177.6	Ⅰ
438	1.48	5.02	2.50	147.6	Ⅱ
439	2.49	5.01	2.50	164.4	Ⅱ

Table 2 Material properties of steel plates.

Plate	Yield Point (σ_y: t/cm^2)	Tensile Strength (σ_u: t/cm^2)	Yield Ratio (σ_y/σ_u)	Elongation (%)
HQ780	5.90~6.94	7.50~8.17	0.79~0.87	11.0~32.0
SS400	2.71~2.85	4.52~4.61	0.59~0.63	27.7~32.0

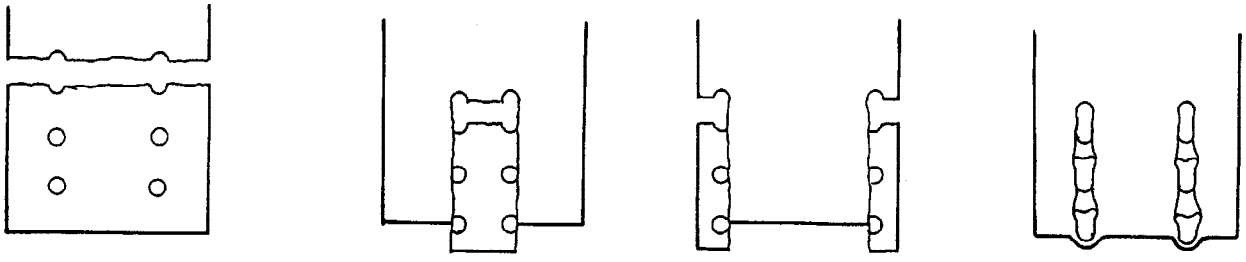

Fig. 1 Failure modes of bolted joint plates.

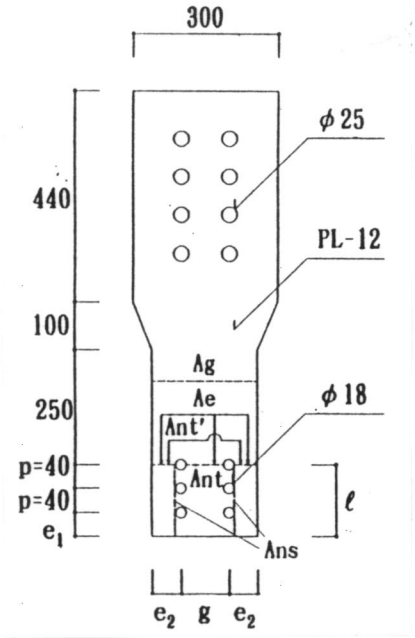

Fig. 2 Test specimen.

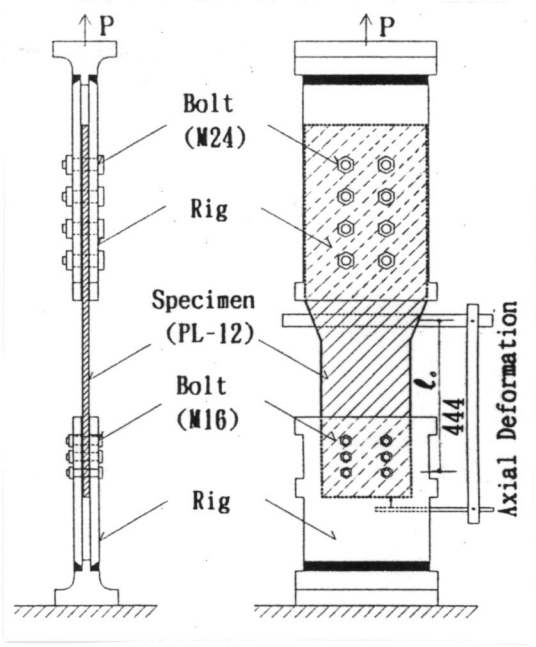

Fig. 3 General view of test apparatus.

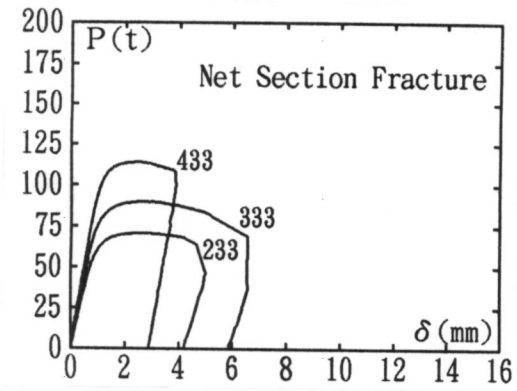

(a) Net section fracture

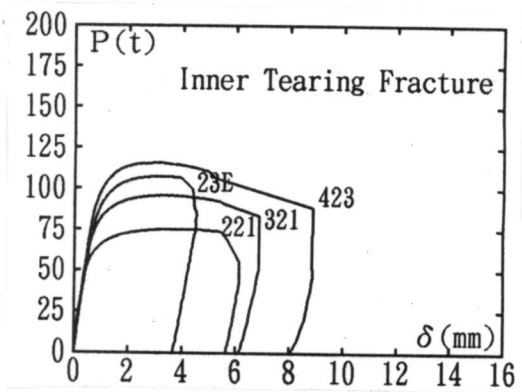

(b) Inner tearing fracture

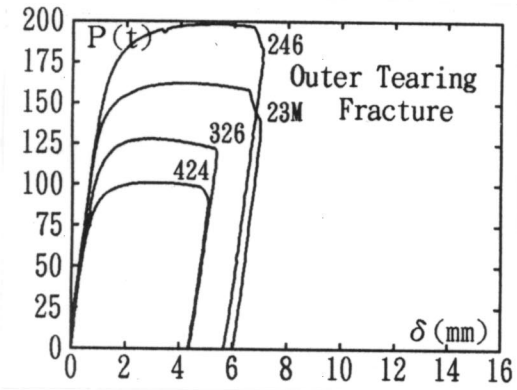

(c) Outer tearing fracture

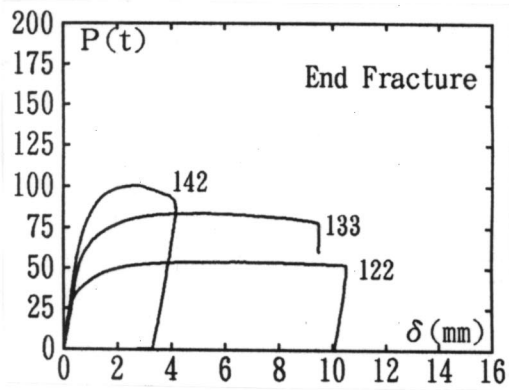

(d) End fracture

Fig. 4 Load and axial deformation.

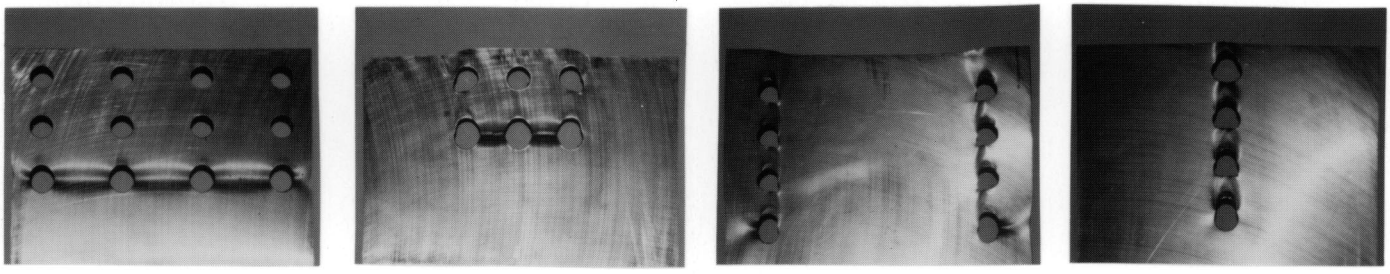

(a) Specimen 433 (b) Specimen 321 (c) Specimen 246 (d) Specimen 142

Photo. 1 Each type of fracture after test.

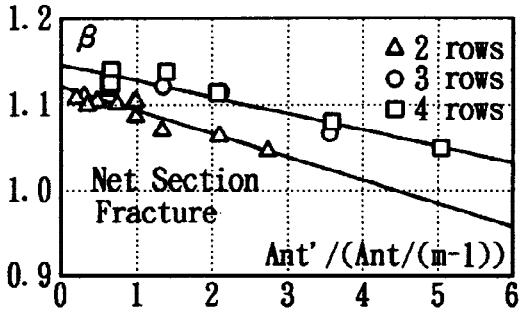

Fig. 5 Increase coefficient of tensile strength.

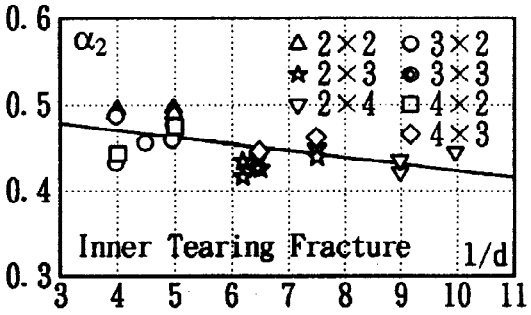

(a) Inner tearing fracture

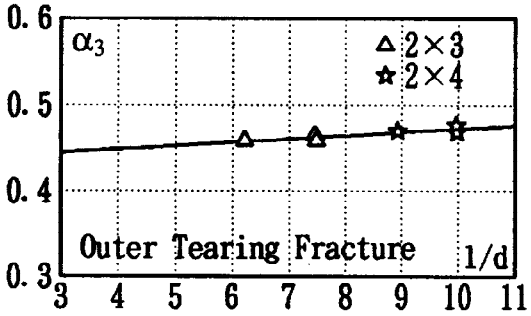

(b) Outer tearing fracture

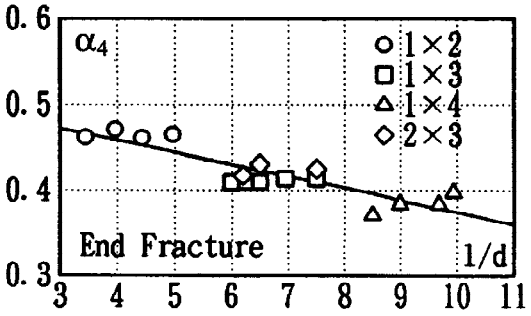

(c) End fracture

Fig. 6 Shear strength coefficient.

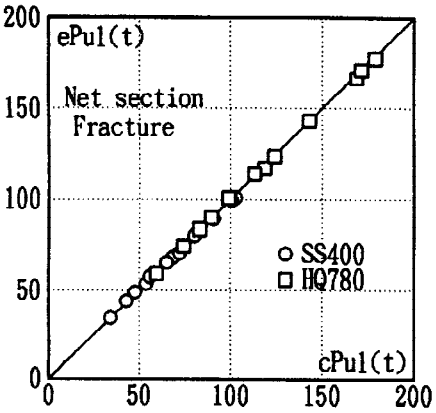

(a) Net section fracture

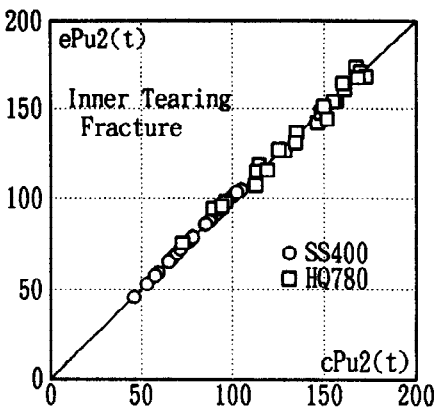

(b) Inner tearing fracture

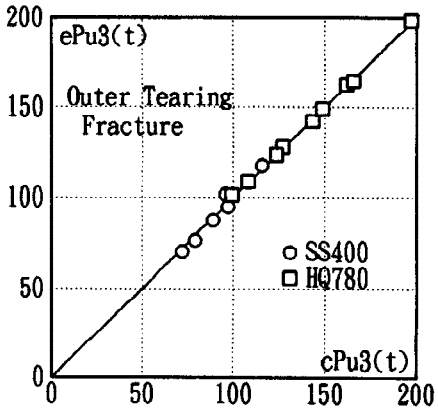

(c) Outer tearing fracture

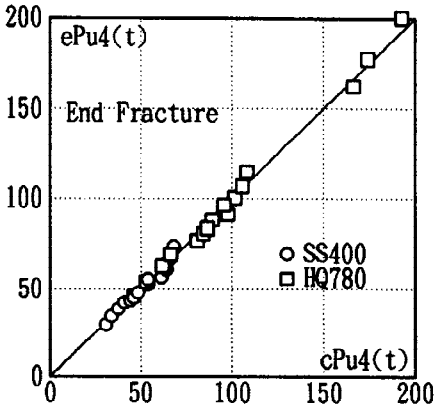

(d) End fracture

Fig.7 Ultimate strengths obtained from prediction formulas and tests.

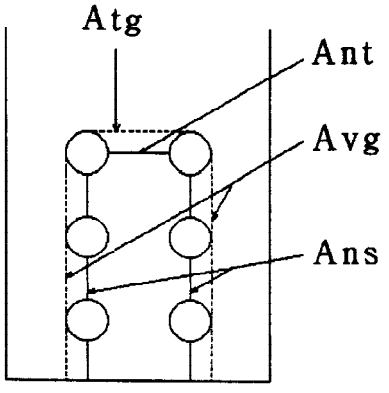

Fig. 8 Section areas in LSD and LRFD.

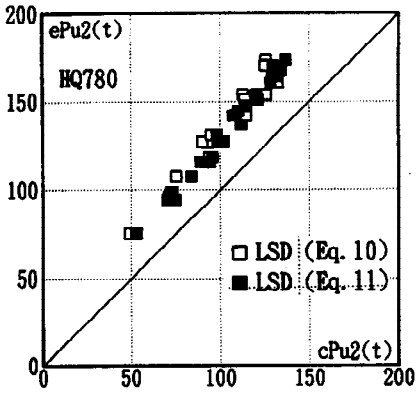

(a) LSD for 780MPa-grade steel

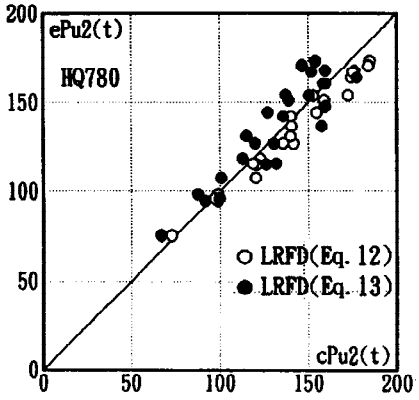

(b) LRFD for 780MPa-grade steel

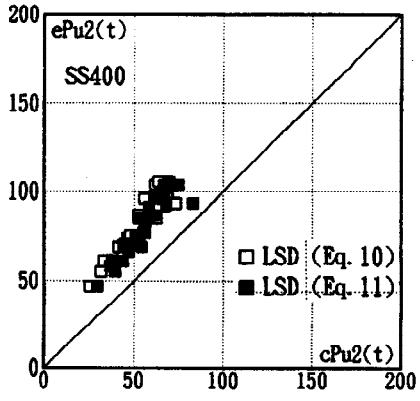

(c) LSD for 400MPa-grade steel

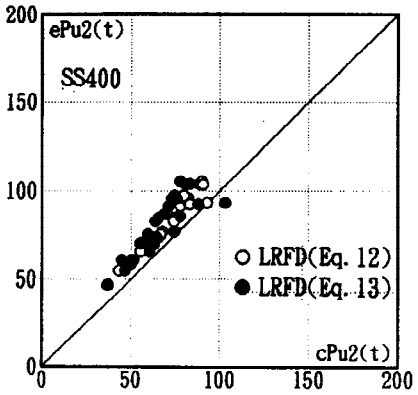

(d) LRFD for 400MPa-grade steel

Fig. 9 Ultimate strengths from test and ultimate strengths in LSD and LRFD.

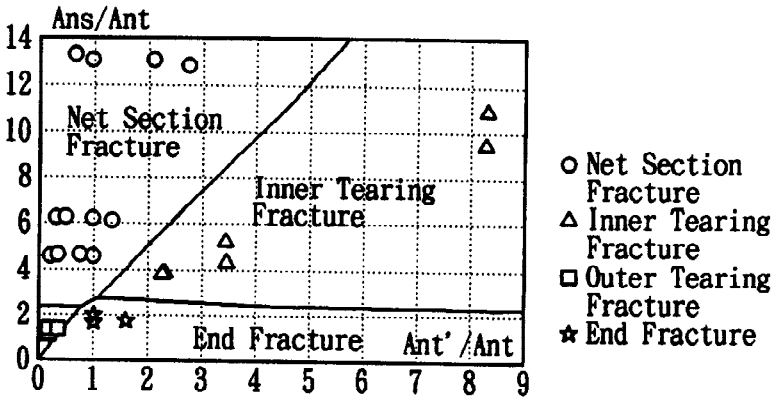

Fig. 10 Fracture domain diagram (2 rows-3 lines).

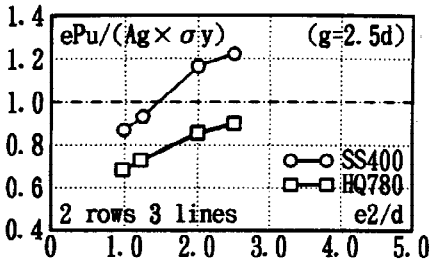

(a) 2 rows and 3 lines

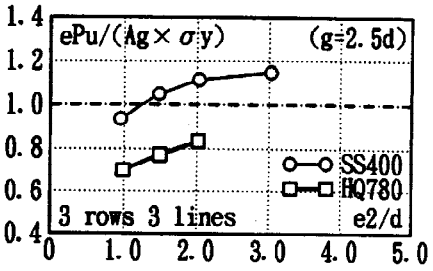

(b) 3 rows and 3 lines

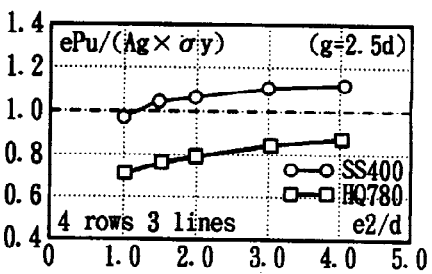

(c) 4 rows and 3 lines

Fig. 11 Edge distance and axial tensile yield force.

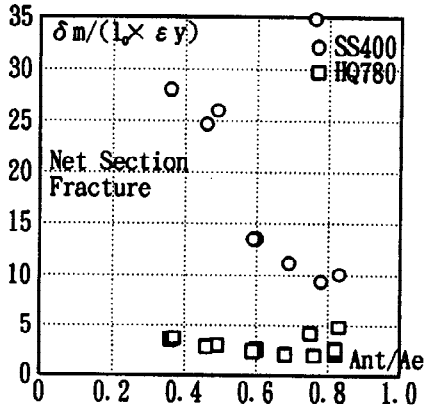

(a) Net section fractur

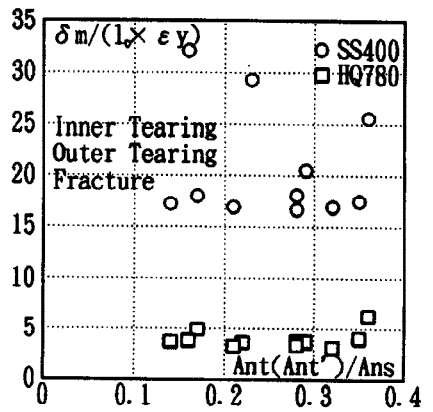

(b) Inner and outer tearing fractures

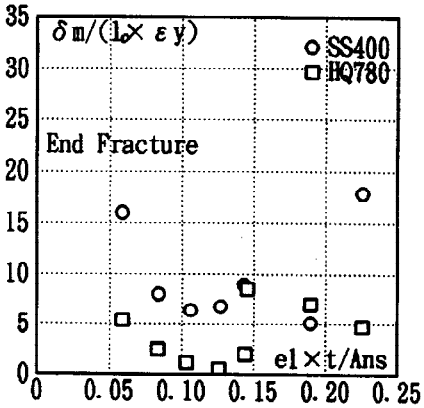

(c) End fracture

Fig. 12 Ductility factors of axial deformation.